Invited Paper

Extraordinary properties of nematic phases of bent-core liquid crystals

A. Jákli[1], M. Chambers[1,2], J. Harden[1], M. Madhabi[2], R. Teeling[2], J. Kim[1] Q. Li[1], G.G. Nair[1,4], N. Éber[3], K. Fodor-Csorba[3], J.T. Gleeson[2], S. Sprunt[2]

[1] *Liquid Crystal Institute, Kent State University, Kent, Ohio 44242, USA*
[2]*Department of Physics, Kent State University, Kent, Ohio, 44242, USA*
[3]*Research Institute for Solid State Physics and Optics, P. O. Box 49, H-1525 Budapest, Hungary*
[4] Centre for Liquid Crystal Research, P.O. Box 1329, Bangalore, 560 0123, India

ABSTRACT

We briefly review systematic and comprehensive studies on several chlorine-substituted bent-core liquid crystal materials in their nematic phases. The results, in comparison to rod-shaped molecules, are both extraordinary and technologically significant. Specifically:

a) Electrohydrodynamic instabilities provide unique patterns including well defined, periodic stripes and optically isotropic structures.
b) Rheological measurements using different probe techniques (dynamic light scattering, pulsed magnetic field, electrorotation) reveal that the ratio of the flow and rotational viscosities are over two orders of magnitudes larger in bent-core than in calamitic materials which proves that the molecule shape and not its size is responsible for this behaviour.
c) Giant flexoelectric response, as measured by dynamic light scattering and by directly probing the induced current when the material is subject to oscillatory bend deformation, turns out to be more than three orders of magnitude larger than in calamitics and 50 times larger than molecular shape considerations alone would predict. The magnitude of this effect renders these materials as promising candidates for efficient conversion between mechanical and electrical energy.
d) The converse of this effect when the bent-core material sandwiched between plastic substrates 4 times thicker than the liquid crystal material provided displacements in the range of 100nm that is sensitive to the polarity of the applied field thus suggesting applications as beam steering and precision motion controls.

1. INTRODUCTION

The discovery of the mesogenic properties of bent-core molecules has opened up a major new and exciting dimension in the science of thermotropic liquid crystals (LCs). Seminal findings – having broad implications for the general field of soft condensed matter – include the observation of ferroelectricity and spontaneous breaking of chiral symmetry in smectic phases composed of molecules that are not intrinsically chiral.[1] To date, most of the research effort has focused on bent-core smectics; liquid phases exhibiting purely orientational order (nematic phases) are rather uncommon in bent-core compounds. However, very recently a number of new bent-core compounds with nematic phases (BCNs) have been synthesized.[2,3,4] Simultaneously there has been a surge in theoretical studies[5,6,7,8] predicting intriguing new thermotropic nematic and isotropic structures. These include biaxial phases, orientationally ordered but optically isotropic phases, and even spontaneously chiral and polar liquid phases; these are all made theoretically possible by the bent shape of the molecules. Moreover, the most ubiquitous and commercially successful LC technology continues to be based on nematics because of the unmatched advantages of fluidity and large response to external forces. Some aspects of this response, such as electric polarization induced by mechanical distortion (so-called flexoelectricity), were found to be particularly enhanced by bent-shaped mesogens.[9] The combination of these factors suggests that BCNs hold significant promise for new and/or improved applications involving soft materials with unprecedented electrical, optical, and/or mechanical responses.

2. MATERIALS STUDIED

We have studied a range of BCN compounds, and here we summarize results on those BCN compounds where the central unit is phenyl with one or two chloro substitutions.

Emerging Liquid Crystal Technologies III, edited by Liang-Chy Chien,
Proc. of SPIE Vol. 6911, 691105, (2008) · 0277-786X/08/$18 · doi: 10.1117/12.768866

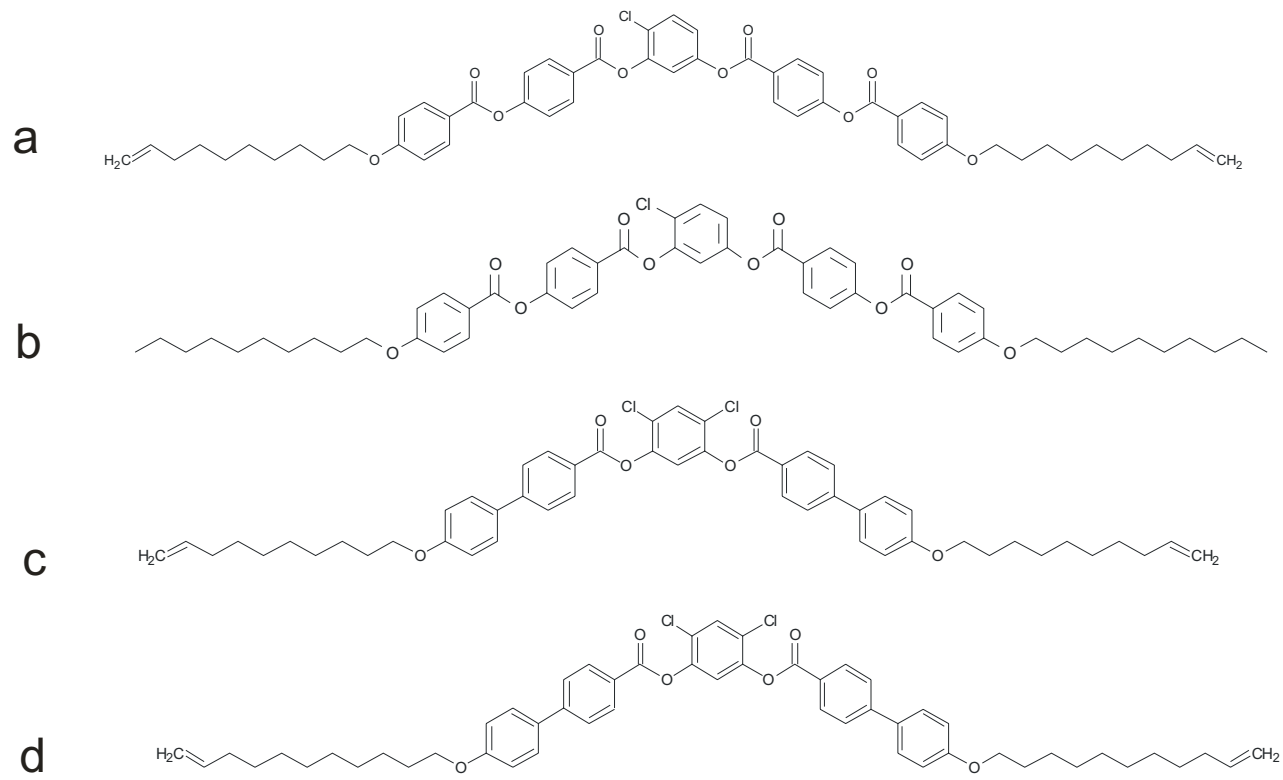

Figure 1: Bent-core materials studied in this paper.

The first and second bent-core compounds 4-chloro-1,3-phenylene bis[4-(10-decenyloxy)benzoyloxy] benzoate *(BCN-a)* and 4-chloro-1,3-phenylene bis[4-(4-n-dodecyloxybenzoyloxy)benzoate] (BCN-b) were re-synthesized in the Synthetic Facility of the Liquid Crystal Institute of Kent State University following the synthetic steps described in Ref.[10] and Ref. [11]. BCN-a exhibits a nematic phase only in cooling between 72°C and 50°C (as the nematic phase is metastable the crystallization depends on the cooling rate and external noise). In this molecule the arms are relatively flexible, because the outer benzene rings are separated by ester groups. It has been the subject of several studies[12,13] and it was shown that although their dielectric and Frank elastic constants ($\Delta\varepsilon$~-1.6, K_{11}~K_{33}~$2.3x10^{-12}$N) and the diamagnetic anisotropy (χ_a=$1.7x10^{-7}$ (SI) are typical for calamitic liquid crystals, the leading Landau coefficient is 30 times lower, the viscosity associated with nematic order fluctuations is 10 times higher[13], the conductivity anisotropy is 2 orders of magnitude lower, and the flexoelectric coefficient is 3 orders of magnitude larger than typically observed in calamitic rod-shaped liquid crystals.[9] BCN-b has the same core as of BCN-a, the "only" difference is that its end-tails are saturated. This difference results in higher isotropic-nematic phase transition temperature and the appearance of an optically isotropic smectic phase[14] with sequence, I - 95°C - N - 80°C - SmC_AP_F.

The other two materials 4,6-dichloro-1,3-phenylene-bis 4-[{4'-(9-decenyloxy))biphenyl] carboxylate (BCN-c) and 4,6-dichloro-1,3-phenylene-bis 4-[{4'-(10-undecenyloxy))biphenyl] carboxylate (BCN-d) have two chlorine units in their central phenyl rings and the aromatic rings of the arms are directly linked making them much more rigid. These differences result in enantiotropic nematic phases in the *97.4°C - 55°C* and the *100.6°C - 51.3°C* ranges, respectively. These materials were prepared by the synthetic routes described in Ref. [15].

The purity of the samples was checked by high performance liquid chromatography (HPLC) using a Merck-Hitachi chromatograph equipped with a Merck RP18 column (Cat. No 16051).

3. RHEOLOGICAL PROPERTIES

We noted that filling sandwich-type cells with these materials via capillary action takes more than an hour instead of less than one minute for calamitic liquid crystals, indicating either anomalously high flow viscosity or unusually weak surface wetting forces. To clarify this we studied both the flow and rotational viscosities of BCN-a.[16] For the rotational viscosity measurements the pulsed magnetic field method[17] was used. For the measurement of the flow viscosities we have chosen a novel 'electro-rotation' technique recently described in smectic liquid crystals[18]. Unlike traditional shear

flow experiments[19,20], this technique requires only a small amount of material, does not rely on uniform alignment over large areas, and allows one to locally probe rheological properties. These advantages are especially important for the study of bent-core nematic materials which are not yet commercially available.

These studies revealed that the viscosities of BCN-a are 1-3 order of magnitudes larger than of calamitic liquid crystals. The rotational viscosity values are more than an order of magnitude larger than in rod-shaped molecules like pentyl-cyanobiphenyl or methoxy benzylidene butyl aniline – the same order of increase that was reported in light scattering studies of director fluctuations[5].

Interestingly electro-rotation measurements that test the flow viscosity under electric fields at very low (<0.1 Hz) frequencies show an even more striking difference between calamitic and bent-core nematics: it is the ratio of rotational and flow viscosities $\Gamma=\gamma_1/\eta$. In calamitic nematics[21] $\Gamma_c\sim10$, whereas in this bent-core material $\Gamma\sim0.02$. This shows that the large shear viscosity is not primarily due to the increased size of the bent-core molecule relative to typical calamitics, but rather due to the shape differences of the molecules. The enormous effective viscosity (~200Pas) measured by the electrorotation technique may also be due to non-Newtonian nature, resembling to Bingham fluids. While rod-shape molecules can translate during shear flow, bent-shape molecules experience a steric barrier to passing by each other. This may promote the formation of temporary clusters, which explains the gooey consistency of the material even in the isotropic phase. Such a clustering has been suggested by several studies[13,22] though the exact size, shape and temporal behavior of the clusters are not known.

3. ELECTROHYDRODYNAMIC INSTABILITIES

Recently, we have documented an unprecedented sequence of instabilities in BCN-a, which cannot be explained by standard models of liquid crystal pattern formation. Instead, our results suggest a connection between these instabilities and the unexpectedly large flexoelectricity. Examples of electric field induced structures near the threshold for the onset for several materials are shown in *Figure 2***.**

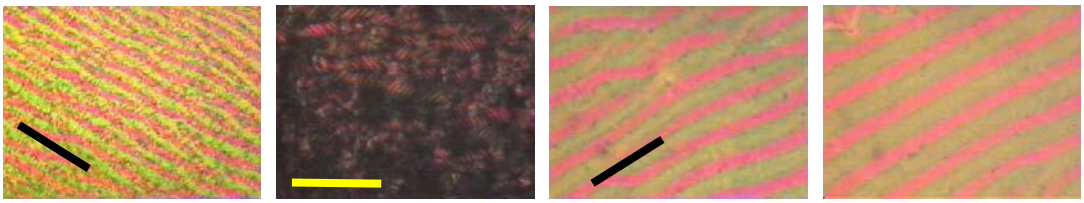

Figure 2: Typical textures near the unset of the hydrodynamic instability. (a and b): 10μm thick BCN-d at 81°C under U=50V, 30Hz with rubbing direction 30° and 0° with the polarizer, respectively. (c and d): 10μm thick BCN-c at 90°C, U=120V under 100 Hz (c) and 500Hz (d). The bars are perpendicular to the rubbing direction, the length corresponds to 50μm.

The pattern shown *Figure 2* strongly resembles the so-called prewavy pattern seen in BCN-a at higher frequencies which are stripes running normal to the director.[12] Typical textures at well above the thresholds in BCN-a are illustrated in *Figure 3*. The regular stripe pattern near the transition were discussed and mainly analyzed in [12], but the pattern under high fields may require completely different approaches. What is most striking is not that the pattern becomes more and more chaotic with smaller and smaller size of compartments until it becomes optically isotropic (see *Figure 3*/f), but rather that it becomes birefringent again at higher fields (see *Figure 3*/g and h) Although presently we do not understand the physical mechanism of this birefringence, it is interesting that the brighter regions in *Figure 3*/g seem to be located at the same places where the disclination lines in *Figure 3*/e. That might suggest that the turbulence did not destroy the singularity around the disclination.

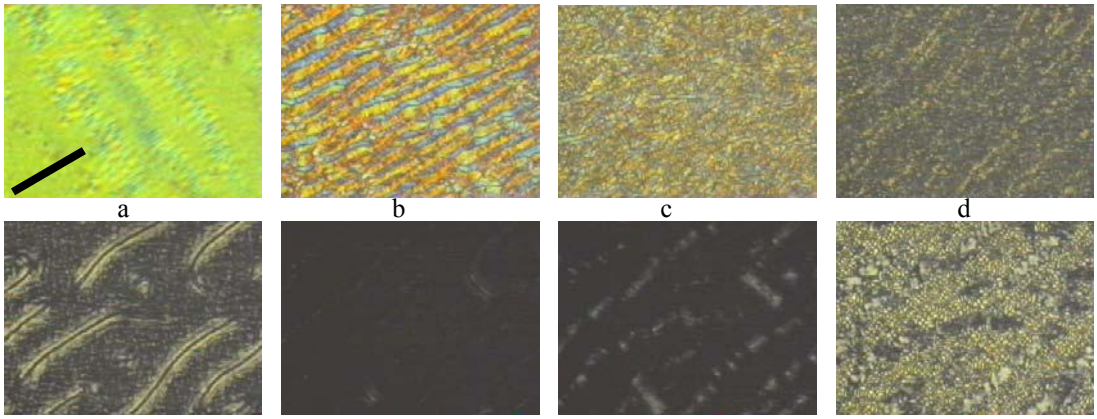

Figure 3: Textures of 10μm BCN-a film at 73°C under 10Hz rectangular fields. a) 30V; b) 45V; c) 60V; d) 80V; e)95V; f) 110V; g) 125V; h) 130V. The orientation of the bar indicate the rubbing direction in all pictures, the length corresponds to 50μm.

4. GIANT FLEXOELECTRICITY

The flexoelectric effect[23,24] (coupling between electric polarization and elastic flexure) yields a polarization, $\vec{P}_f$ in normally apolar nematic LC when the average direction for orientational order or director, $\vec{n}$ is subjected to splay or bend deformations. The effect is enhanced for molecules which possess a permanent dipole moment and shape anisotropies, specifically for pear-shaped or banana-shaped molecules. In these cases (see Figure 4a), orientationally deformed structures having nonzero $\vec{P}_f$ have both closer molecular packing and lower free energy than non-polar arrangements.

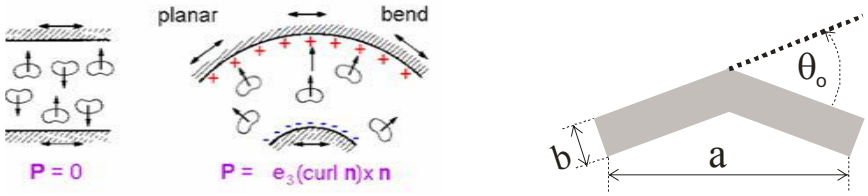

a b

Figure 4: (a) Illustration of the dipolar mechanism of flexoelectricity for bent-core (banana shape) liquid crystals. Model of the bent-core molecules used in microscopic theory.

The flexoelectric polarization of a standard uniaxial nematic LC can be expressed in terms of two flexoelectric coefficients e_1 and e_3, corresponding to splay and bend deformations, respectively, such as shown in Eq.(1).

$$\vec{P}_f = e_1\vec{n}\left(\vec{\nabla}\cdot\vec{n}\right) + e_3\left(\vec{\nabla}\times\vec{n}\right)\times\vec{n} \qquad (1)$$

A molecular – statistical approach for calculating the flexoelectric coefficients was subsequently developed by Helfrich[25]. This model states that the bend flexoelectric constant e_3 can be related to the kink angle θ_o as:

$$e_3 = \frac{\mu_\perp K_{33}}{2k_B T}\theta_o\left(\frac{b}{a}\right)^{2/3} N^{1/3} \qquad (2)$$

In this expression $\mu_\perp$ is the molecular dipole moment along the kink direction, a, and b are length and width of the molecules, θ_o is the kink angle (Figure 4/b), T is the absolute temperature and N is the number density of the molecules. Helfrich's approach assumes that the molecules have no positional ordering, i.e. the molecules fluctuate independently. For rod-shaped molecules θ_o<1°; however for typical banana-shaped molecules θ_o~60°. In conventional rod-shaped nemat-

ics, the flexoelectric coefficients are typically 10^{-11}-10^{-12}C/m; based on Helfrich's model, we estimate that BCNs may have coefficients ~50 times greater. Recently some of us were testing this effect in BNC-a by a direct method via measuring the electric current produced by periodic mechanical flexing of the NLC's bounding surfaces.[9] These results revealed that the bend flexoelectric coefficient is more than three orders of magnitude larger than in calamitics, i.e., much larger than would be expected from Helfirch's microscopic model based on molecular geometry. This is especially interesting, because with this large coupling bent-core nematic (BCN) materials can form the basis of a technological breakthrough for conversion between mechanical and electrical energy.

To test how general is this giant flexoelectricity among bent-core liquid crystals we have further improved the direct flexing setup, and employed dynamic light scattering technique to independently measure the flexoelectric coefficients on all the bent-core materials and their mixtures listed in paragraph 2.

Finally, we have also attempted to measure the converse of this effect, i.e. the electric field induced flexing. In the remaining of this paper we are describing these techniques and summarize the main preliminary results.

4.1 Direct flexoelectricity measured by flexing method

To flex the LC cell, a custom made setup was created as shown in Figure 5. Essentially the LC cell is periodically flexed and the induced current is resolved at the flexing frequency by a lock-in amplifier. An electric motor and transmission are used to provide rotational motion which is converted to lateral (pure z axis) motion via a scotch yoke. The flexing LC cell is connected to the lock-in where the reference signal is provided by an optical sensor on the moving scotch yoke. The transmission allows control of flexing frequency. Additionally end pieces for the motor allow the change of the displacement amplitude S_0 from 0.5 to 4 mm, in 0.5 mm increments. The temperature holder is isolated from the table and heated on both the top and bottom faces, with temperature sensors located at the top and bottom of the holder. A PID temperature controller controls the heating. A third temperature sensor located near the sample is used for measurement of the sample temperature. The lock-in technique allows the magnitude of the induced RMS current, I_{RMS}, on the cell to be measured precisely as function of temperature, T, displacement amplitude, S_0 and frequency, ω. Therefore, $e_3|$ may be calculated from this I_{RMS}.

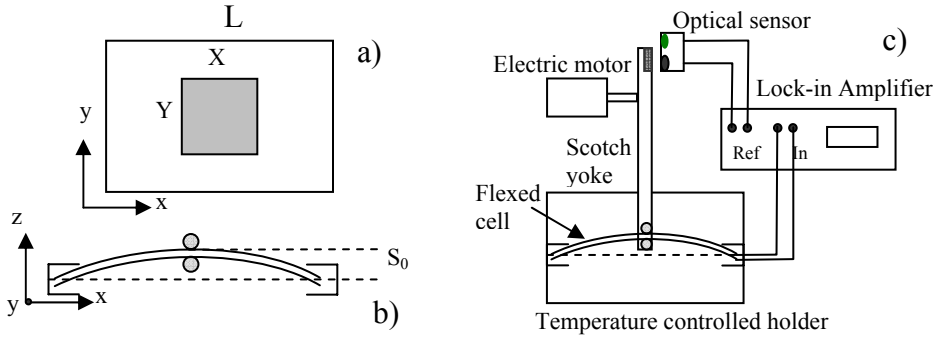

Figure 5: Illustration of the modified experimental set-up used to measure the flexoelectricity by flexing the cells and measuring the induced electric current. (a): cell description, (b): cell holder, (c): experimental set-up.

This setup is different from the one used previously by Harden et al.[9] in a number of respects:

(i) The flexing is not supplied by a speaker which requires a driving with the same frequency electric signal where the measurements are performed, but is driven by a DC motor, so the background signal is minimized.

(ii) The amplitude of the flexing is not changing with frequency, but is constant in the 1-30Hz range set by the eccentric end-pieces.

(iii) The exact position of the motor could be adjusted by a set of micro-positioners, thus one could set the S_o=0 before the measurements to minimize the influence of the quadratic signal on the first harmonic.

(iv) During the flexing the end of the cell is not fixed, but is able to flex. This change in the flexing profile is important, because it provides uniform buckle (avoid electrical shortage during flexing) and is able to withstand repeated deformation (on the order of 1 x 10^5 oscillations / measurement). It also simplifies the analysis of the profile, which now

can be well approximated by an arc, and for small displacement S_o<<X, the bend flexoelectric constant can be related to the measured electric current I_{RMS} and the geometrical parameters of the flexing cells, as

$$|e_3| = \frac{\sqrt{2} I_{RMS} L^2}{8 A \omega S_0} \qquad (3)$$

In this expression A (= XY) is the active (electrode covered) area that is distorted out of plane at an angular frequency, ω by a distance S_0 , and L is the width of the cell including non-electrode areas.

In the previous measurements thin sheet brass plates and ITO coated Mylar films were used. Brass, although robust doesn't allow patterned electrodes; ITO coatings on plastics tends to fracture under repeated bending. Fortunately, conducting polymers do not degrade as quickly as ITO. For this reason typically in our measurements an organic conducting polymer coated substrate with a thickness of around 60 μm was patterned. For alignment poly vinyl alcohol (PVA) was coated onto the substrate and subsequently rubbed. Usually, a Mylar sheet spacer of around 100 μm was used, where the active area contained multiple compartments to reduce electrical shorts and material escaping during flexing.

The sample is loaded at low temperature and heated to the isotropic phase. A temperature ramp from isotropic to crystal is then performed at a rate of around 1-2 ^{o}C/min. The typical frequency range is on the order of 3-6 Hz with S_0 = 1 – 2 mm.

For each samples we have measured the temperature dependence of the Differential Scanning Calorimetry (DSC) signals, the optical transmission and the flexoelectric coefficient. An example of such curves is shown in Figure 6 for BCN-a. One can see that the giant flexoelectric signal sets up at the isotropic-nematic transition, but its range appears to be narrower than of the nematic range measured with DSC and optical transmission. This is due to the monotropic (metastable) nature of the nematic phase, which becomes unstable under mechanical flexing, but is more stable in the other two measurements that do not involve mechanical disturbance.

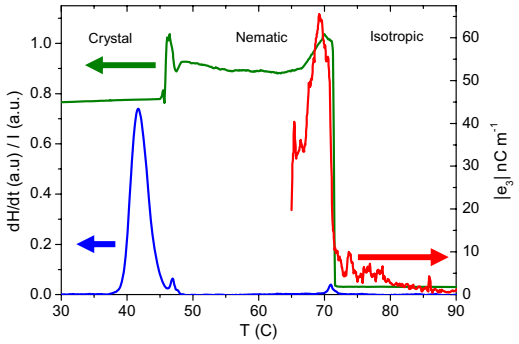

Figure 6: Measurement of the flexoelectricity (|e_3|, red), Differential Scanning Calorimetry (dH/dt, blue) and optical intensity of an unaligned film between crossed polarisers (green) of the bent-core material.

Details of the measurement on the other bent-core materials and on their mixtures will be published separately.[26] It was found that the mono-chloro materials (BCN-a and b) have larger flexoelectric coefficients than of the dichloro substituted materials, but although even their values are larger than 10nC/m. It is also important to mention that some binary and ternary mixtures of these materials have wide nematic temperature range including room temperature, thus making the application of the giant flexoelectricity realistic.

4.2 Dynamic light scattering study of flexoelectricity

Dynamic light scattering provides an alternative means to characterize flexoelectricity in BCNs without the need for externally applied forces. Since fluctuations in electric polarization are coupled to director fluctuations through the flexoelectric coefficients e_1 and e_3, one expects a modification of the standard nematic director modes due to flexoelectricity. The details were first worked out by the Orsay group[27]. Starting from the phenomenological definition of the flexoelectric polarization, and utilizing the expression for the nematic elastic free energy and relevant results from electrostatics, they obtained the following results for the intensity (I) of light scattered from nematic fluctuation modes and their associated relaxation rates (Γ),

$$I_1 \propto \frac{(\Delta\varepsilon)^2 k_B T}{K_1 q_x^{\,2} + K_3 q_z^2 + e^2 q_x^{\,2} q_z^2 / (\varepsilon_\perp q_x^{\,2} + \varepsilon_\parallel q_z^2)}$$
$$\Gamma_1 = \frac{K_1 q_x^{\,2} + K_3 q_z^2 + e^2 q_x^{\,2} q_z^2 / (\varepsilon_\perp q_x^{\,2} + \varepsilon_\parallel q_z^2)}{\eta_1} \qquad (4)$$
$$I_2 \propto \frac{(\Delta\varepsilon)^2 k_B T}{K_2 q_x^{\,2} + K_3 q_z^2}$$
$$\Gamma_2 = \frac{K_2 q_x^{\,2} + K_3 q_z^2}{\eta_2}$$

Here the subscripts 1,2 on the left hand side refer to splay-bend (elastic constants K_1, K_3) and twist-bend (K_2, K_3) normal modes. The corresponding viscosities η_1, η_2 are the usual wave vector (**q**)-dependent combinations[28] of the various fundamental viscosities of a nematic fluid. The scattering wave vector is taken as **q** = (q_x, q_z), where z corresponds to the direction of the average (aligned) director. The quantities $\varepsilon_\parallel$, $\varepsilon_\perp$, and $\Delta\varepsilon$ are, respectively, the principal dielectric constants parallel and perpendicularr to the director and dielectric anisotropy of a uniaxial nematic, and $e = e_1 + e_3$.

The results above reveal that only the amplitude and dispersion of the splay-bend mode (mode 1) are affected by flexoelectricity. Therefore, to probe the latter one needs to select a scattering geometry that isolates mode 1. It is then convenient to choose either $q_x = 0$ or $q_z = 0$. Rocking **q** off this choice, one expects from Eq. (4) a parabolic dispersion about a local minimum in I_1^{-1} or Γ_1 whose curvature is determined either by the combination $K_1 + e^2/\varepsilon_\parallel$, or by $K_3 + e^2/\varepsilon_\perp$. However, when e^2 is *very* large (as previously determined by the electromechanical method for BCN-a[9]), the mode 1 amplitude will be very weak – and the magnitude of the flexoelectricity very challenging to measure reliably – except when $q_x = 0$ or $q_z = 0$ to high accuracy. Thus, great demands are placed on high quality director alignment and high experimental **q** resolution.

We performed out light scattering study on 10 micron thick cells containing the compound BCN-a and its dichloro analog BCN-c at temperatures ~2°C below the isotropic-nematic transition[29] . The surfaces of the sample cells were treated for homogeneous planar director alignment. To isolate mode 1, we used the scattering geometry presented in Fig. 1. Here the incident and detected scattered light polarizations, and the aligned director, all lie in the horizontal (*H*) scattering plane (*HHH* geometry). The time correlation function of the scattered light intensity was recorded as a function of q_x about $q_x = 0$ for essentially fixed $q_z = 99300$ cm^{-1}. The correct orientation of the director was carefully checked by placing a crossed analyzer in the forward direction and rotating the sample to produce a minimum in transmitted light. In the event, only slowly fluctuating light was observed through the analyzer at **q** ≈ 0, confirming uniform orientation of the director in the scattering plane. In spite of our best efforts to obtain a pure *HHH* scattering geometry (Fig. 1), for which scattering from mode 2 should vanish[28], we still detected a contribution from mode 2 fluctuations. This is a reflection of both very large flexoelectricity, which, according to Eq.(4), selectively suppresses scattering from mode 1, and finite experimental **q** resolution.

From fitting the measured correlation functions to a double exponential decay (corresponding to overdamped modes 1 and 2), we extracted Γ_1 and Γ_2, and confirmed a parabolic dispersion of Γ_1 about $q_x = 0$ and for finite q_z, with a large curvature indicative of a large value of $e = e_1 + e_3$ in both materials studied. To obtain the magnitude of e, we calculated the ratio

$$\frac{\Gamma_1}{\Gamma_2} \approx 1 + \left(\frac{K_1}{K_3} + \frac{e^2}{\varepsilon_\parallel K_3} \right) \frac{q_x^{\,2}}{q_z^{\,2}} \qquad (5)$$

for small q_x (where $\eta_1 \approx \eta_2$). Fitting this to a parabolic dispersion in q_x and using previously determined values of the parameters K_1, K_3 and $\varepsilon_\parallel$, we obtain e = 90 nC/m in BCN-a and e = 20 nC/m in BCN-c. These values have the same order of magnitude as determined from electro-mechanical measurements of the flexoelectricity in these compounds at similar nematic temperatures, and therefore provide an independent confirmation of the giant flexoelectric effect in BCNs.

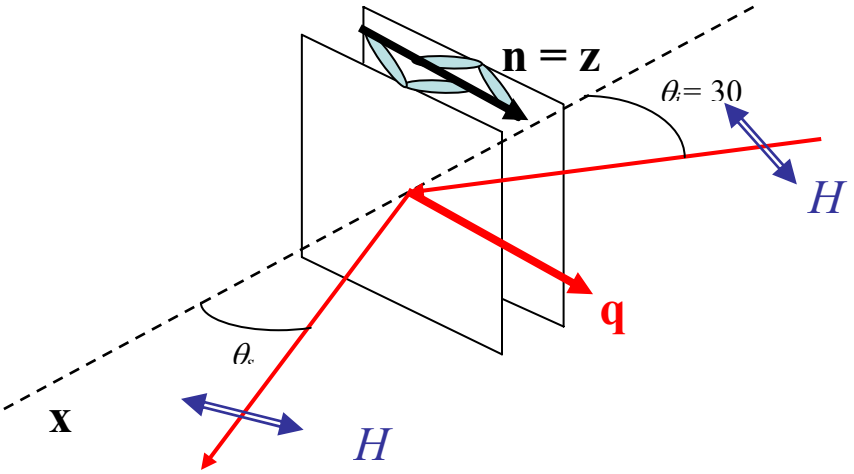

Figure 7: Geometry of our light scattering experiment. Two bent-core molecules are indicated in light blue. Red arrows represent the directions of incident and scattered (detected) laser light. The aligned director ***n*** *(black arrow) lies along the z direction in the x-z scattering plane. Incident and scattered polarizations, lying in the horizontal (H) scattering plane, are depicted by blue double arrows.* q_x *scans about* $q_x = 0$ *(and for essentially fixed* q_z *) are conducted by varying the scattering angle* θ_s *over values very close to* $\theta s = -\theta_i = -30°$ *(for fixed incident angle* θ_i*).*

4.3 Converse Flexoelectricity

With the discovery of giant flexoelectricity, materials and methods may be produced that allow for practical utilization of the converse flexoelectric effect, that is, producing a flexing of a film when an electric field is applied. According to our best knowledge, converse flexoelectricity has never been observed in thermotropic liquid crystals. In lyotropic liquid crystals, the first observation was on black bilayer lipid membranes which produced a $20m^{-1}$ curvature[30,31,32]. However, these are susceptible to rupture and the membranes had to be submerged in an aqueous solution. Lipids have a large e_1 (splay flexoelectric coefficient)[33] on the order of 100pC/m which will produce curvature about 2 axis whereas the BCNs have a large e_3 (bend flexoelectric coefficient) on the order of 100nC/m which produces curvature about 1 axis.

So far we have measured the converse flexoelectric effect of BCN-a.[34] The samples were constructed by using two 100µm thick Mylar substrates with ITO sputtered as a conducting layer. Polyvinyl alcohol was spin coated and rubbed as an alignment layer. The overall size of the sample was 14mm x 21mm, while the electrode region was 12mm x 18mm and the cell gap was set to 25µm by glass fiber spacers sparsely distributed throughout the region.
The material BCN-a was capillary filled into cells constructed from these substrates. The sample rested on two 2mm diameter glass rods which were mounted in an Instec Hot stage HS 2000 regulated by an Instec Heat Controller. The electrical leads of the sample was connected to a BK Precision DC Power Supply and a 10 times voltage amplifier. Voltage was measured with an HP 34401A multimeter.
A Leitz Mirau Interferometer mounted to the bored and rethreaded objective port of an Olympus BX51 Microscope (in reflection mode) was used to measure the upward or downward deflections of the sample. Figure 8 gives a schematic of the experimental apparatus. The interferometer was adjusted such that 3 to 5 fringes were viewable on the video display. Images were recorded at 0V and about 2 seconds after the voltage was applied.
When voltage was supplied to the sample, the fringes would shift left (an upward displacement) or right (a downward displacement). This motion can be verified by using the fine adjustment of the microscope focus. Moving the stage slightly up yielded fringes that shifted left. Moving slightly down yielded right shifts. A green filter (532nm) was used to improve the contrast of the fringes. The theoretical accuracy limits for an interferometer is 3 nm[35], however, vibrations and thermal fluctuations in this set up extended this limit to about 5nm when mounted on a vibration damped optics table, which was still much smaller than the experimentally observed deflections in the 10nm to 200nm range.

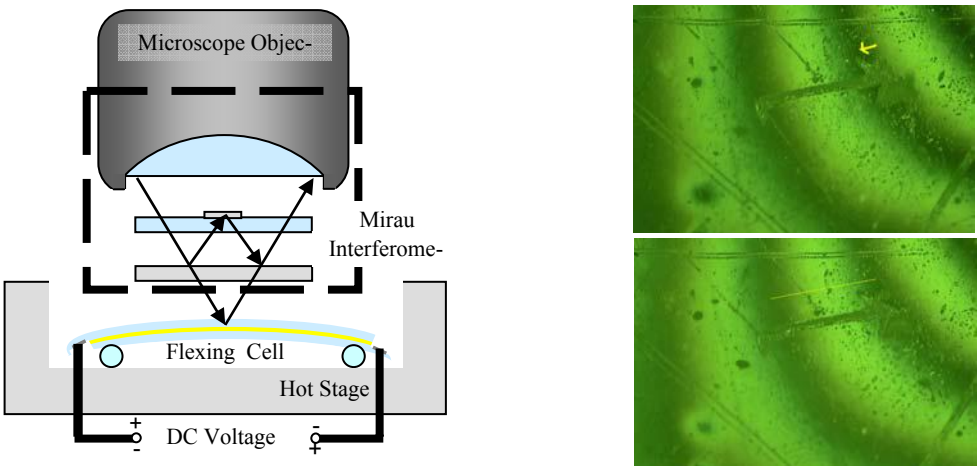

Figure 8: The set-up (left) and the typically observed fringe shifts corresponding to an upward deflection (right).

For each of the experiments applied voltage, temperature, upward or downward deflection and the position where the sample viewed along the length of the cell was measured. Of the four measurable quantities, only deflection could not be measured directly.

We have measured the distance from fringe to fringe in pixels noting which direction the fringes have shifted through time and the fringe shift in pixels. The arrow in Figure 8 tells not only the fringe shift in pixels but the direction as well. This shift can be converted to an actual displacement, l, by the formula $l=m\lambda/2n$, where m is the relative fringe displacement that is, the ratio of the fringe shift to the distance between fringes. λ is the wavelength (532nm) and n is the index of refraction which in this case is n=1 since we are in air. With this we measured the deflections under positive and negative potential differences at the function of temperature, position and applied voltage. From this we were able to calculate the flexoelectric coefficient e_3 by assuming that the converse flexoelectric energy is compensated by the bend energy of the Mylar with Young modulus Y~3.3GPa[36]. Our calculations[34] show that e_3 ~50nC/m, i.e., basically the same value which was measured from the direct effect[9].

One specific application of the direct flexoelectric effect, with a very large market potential, would be personal electric power generators run by ordinary body movements - e.g., a wearable flexoelectric film that would convert mechanical energy developed during ordinary walking or elbow movements into an electric potential for charging personal electronics. Biocompatible versions of these elastomers could also be used in conjunction with medical implants such as pacemakers. The converse of the effect maybe used for mechanical actuators and in beam-steering applications, when simple and light weight devices are needed for small, but very precise steering.

Acknowledgement:
The work was partially supported by NSF-DMR-0606160, the Hungarian Research Grant OTKA-K-61075 and ONR-N00014-07-1-0440.

REFERENCES

[1] T. Niori, T. Sekine, J. Watanabe, T. Furukawa, H. Takezoe, *J. Mater. Chem*. **6(7)**, 1231-1233, (1996); T. Sekine, T. Niori, M. Sone, J. Watanabe, S.W. Choi, Y. Takanishi, H. Takezoe, *Jpn. J. Appl. Phys*., **36**, 6455 (1997); D.R. Link, G. Natale, R. Shao, J.E. Maclennan, N.A. Clark, E. Körblova, D.M. Walba, *Science* **278**, 1924-1927 (1997)

[2] J. Matraszek, J. Mieczkowski, J. Szydlowska, E. Gorecka, *Liq. Cryst.,* **27**, 429-436 (2000); I. Wirth, S. Diele, A. Eremin, G. Pelzl, S. Grande, L. Kovalenko, N. Pancenko, W. Weissflog, *J. Mater. Chem.,* **11**, 1642-1650 (2001); W. Weissflog, H. Nádasi, U. Dunemann, G. Pelzl, S. Diele, A. Eremin, H. Kresse, *J. Mater. Chem,* **11**, 2748-2758 (2001);

[3] E. Mátyus, K. Keserű, *J. Mol. Struct*., **543**, 89 (2001);

[4] T.J. Dingemans, E.T. Samulski, *Liq. Cryst.,* **27**, 131-136 (2000)

[5] A. Roy, N.V. Madhusudana, P. Toledano, A.M. Figureiredo Neto, *Phys. Rev. Lett*., **82**, 1466-1469 (1999);

[6] H.R. Brand, P.E. Cladis, H. Pleiner, *Eur. Phys. J. B*, **6**, 347-352 (1998)
[7] T.C. Lubensky, L. Radzihovsky, *Phys. Rev. E,* **66**, 031704-1-27 (2002); L. Radzihovsky and T. C. Lubensky, *Europhys. Lett.* **54**, 206-212 (2001).
[8] H. R. Brand, H. Pleiner, and P. E. Cladis, *Eur. Phys. J. E*, **7**, 163-166 (2002).
[9] J. Harden, B. Mbanga, N. Éber, K. Fodor-Csorba, S. Sprunt, J.T. Gleeson, A. Jákli, *Physical Review Letters, 97, 157802 (2006)*
[10] K. Fodor-Csorba, A. Vajda, G. Galli, A. Jákli, D. Demus, S. Holly, E. Gács-Baitz, *Macromol. Chem. Phys.,* **203**, 1556-1563 (2002) and K. Fodor-Csorba, A. Jákli, G. Galli*, Macromolecular Symposia* **218**, 81-88 (2004)
[11] G. Pelzl, A. Eremin, S. Diele, H. Kresse, W. Weissflog, *J. Mater. Chem.*, **12**, 2591 (2002); W. Weissflog et al., *Liq. Cryst*., **31**, 923 (2004)
[12] D. B. Wiant , J. T. Gleeson, N. Éber , K. Fodor-Csorba , A. Jákli , T. Tóth-Katona, *Phys. Rev., E* **72**, 041712 (2005)
[13] D. Wiant, S. Stojadinovic, K. Neupane, S. Sharma, K. Fodor-Csorba, A. Jákli, J. T. Gleeson, S. Sprunt, *Phys. Rev. E* **73**, 030703 (R) (2006)
[14] G. Liao, S. Stojadinovic, G. Pelzl, W. Weissflog, S. Sprunt, A. Jákli, *Physical Review E,* **72** 021710 (2005)
[15] K. Fodor-Csorba, A. Vajda, C. Slugovc, G. Trimmel, D. Demus, E. Gács-Baitz, S. Holly, G. Galli, *J. Mater. Chem.*, **14**, 2499-2506 (2004)
[16] E. Dorjgotov, K. Fodor-Csorba, J.T. Gleeson, S. Sprunt, A. Jákli, Liq. Cryst., in print (2008)
[17] Pieranski, P., Brochard, F., Guyon, E., *J. Phys.*, **34**, 35, 1972; de Gennes, P.G., Prost, J., *The Physics of Liquid Crystals*, Oxford University Press, Oxford (1993)
[18] Liao, G., Smalyukh, I. I., Kelly, J. R., Lavrentovich, O.D., Jákli, A., *Phys. Rev. E.,***72**, 031704 (2005),.
[19] Horn, R.G., Kleman, M., *Ann. Phys. (Paris)*, **3**, 229 (1978); Battacharya, S., Letcher, S.V., *Phys. Rev. Lett.* **44**, 414 (1980)
[20] Larson, R. G., *The Structure and Rheology of Complex Fluids*, Oxford university Press, 1999
[21] Merck catalogue 'Liquid Crystal Mixtures for electro-optic displays', EM. Industries, Inc. (1994)
[22] Domenici, V., Veracini C.A., and Zalar, B., *Soft Matt*., **1**, 408 (2005); Cinacchi, G., and Domenici, V., *Phys. Rev*. E, **74**, 030701 (2006)
[23] R. B. Meyer, *Phys. Rev. Lett.*, **22**, 918 (1969).
[24] P. G de-Gennes and J. Prost, The physics of liquid crystals, second edition p.135 , Oxford science publications, Oxford, 1993
[25] W. Helfrich, "A simple method to observe the piezoelectricity of liquid crystals", *Phys. Lett.,* **35A**, 393-394 (1971)
[26] M. Chambers, J. Harden, J.T. Gleeson, S. Sprunt, A. Jákli, in preparation (2008)
[27] Orsay Group, in *Liquid Crystals and Ordered Fluids*, Plenum Press (1970), p. 195
[28] P. G. deGennes and J. Prost, *The Physics of Liquid Crystals* (Oxford, Oxford University Press, 1993), Chapter 4.
[29] M. Majumbdar, K. Neupane, J. Gleeson, A. Jakli, and S. Sprunt, to be submitted.
[30] Todorov, A. T., A. G. Petrov, et al. (1994). "1st Observation of the Converse Flexoelectric Effect in Bilayer-Lipid Membranes." Journal of Physical Chemistry **98**(12): 3076-3079.
[31] Petrov, A. G., M. Spassova, et al. (1996). "Flexoelectricity and photoflexoelectricity in model and biomembranes." Thin Solid Films **285**: 845-848.
[32] Petrov, A. G. (2006). "Electricity and mechanics of biomembrane systems: Flexoelectricity in living membranes." Analytica Chimica Acta **568**(1-2): 70-83.
[33] Derzhanski, A., A. G. Petrov, et al. (1990). "Flexoelectricity of Lipid Bilayers." Liquid Crystals **7**(3): 439-449.
[34] J. Harden, R. Teeling, J.T. Gleeson, S. Sprunt, A. Jákli, in preparation
[35] O. Kafri, *Optics Letters,* **14**(13): 657- 658 (1989)
[36] K. Matsuzawa, *The Journal of the Acoustical Society of Japan* **15**(3), 147-150 (1959).